

# Scattering at sidewall roughness in photonic crystal slabs

Wim Bogaerts, Peter Bienstman, and Roel Baets

Department of Information Technology, Ghent University–Interuniversity Microelectronics Centre,  
Sint-Pietersnieuwstraat 41, 9000 Gent, Belgium

Received November 13, 2002

We have simulated the effect of sidewall roughness in photonic-crystallike structures with different vertical refractive-index contrast. We treated the scattering off a sidewall irregularity as a radiating dipole excited by the incident waveguide mode. We show that the loss that is due to this scattering is significantly larger for structures with a low refractive-index contrast (such as GaAs/AlGaAs waveguides) than for structures with a high vertical index contrast (such as silicon-on-insulators and membranes). © 2003 Optical Society of America

OCIS codes: 250.5300, 290.5880.

One application of two-dimensional (2-D) photonic crystals is in planar waveguide structures. In photonic crystal slabs, light is controlled in plane by a 2-D photonic crystal, e.g., a lattice of holes, whereas vertically, light is guided conventionally by a high or a low refractive-index contrast.<sup>1,2</sup> Normally, the vertical confinement is not perfect; light leaks into the cladding. These out-of-plane losses are closely related to the layer structure and have several causes.

Even perfect photonic crystal slabs can have intrinsic scattering losses when the Bloch modes are not fully confined,<sup>3</sup> although lossless Bloch modes can exist in particular designs.<sup>4</sup> It has been shown that these losses increase dramatically with higher refractive-index contrast between the slab core and cladding.<sup>5</sup> Therefore one can choose low refractive-index contrast, such as in GaAs/AlGaAs system. Although this structure is not lossless, losses can be kept within reason. Alternatively, high refractive-index contrast, as in a silicon-on-insulator structure, can support lossless modes in a photonic crystal.<sup>4</sup> However, a breach in periodicity can cause large scattering losses. Therefore, which material is best for low intrinsic losses depends on the application.<sup>6</sup>

Intrinsic losses give only a lower limit of the overall losses. In real structures, which are often fabricated by lithography and dry etching, additional scattering occurs at sidewall irregularities. Again, we expect the vertical layer structure to play a role. We studied the general effect of the vertical index contrast on these scattering losses by modeling sidewall irregularities as radiating dipoles excited by the guided light. In our 2-D approximation we use air slots in a slab waveguide (Fig. 1, inset). The simulations were made for TE polarization ( $E$  field parallel to the layer interfaces) at 1550 nm. The total power lost that is due to roughness at the sidewall will be proportional to the power loss of an irregularity averaged over any position  $y$  of that irregularity along the interface:

$$L_{\text{tot}} \sim \int P(y)L(y) dy, \quad (1)$$

where  $P(y)$  is the scattered power of the dipole at position  $y$  and  $L(y)$  is the fraction of that power that is not recaptured by the waveguide. Although scattering at irregularities should be treated in a coherent way, we can use this incoherent integration as a figure of merit,

as the irregularities can be distributed randomly on the sidewall. The scattering dipole is excited by the incident field, so its power  $P(y)$  can be written as a function of the local field  $E(y)$ :

$$P(y) = \eta^2(y) \frac{E^2(y)}{2Z_{\text{rad}}(y)}, \quad (2)$$

where  $\eta(y)$  describes the effect of the roughness geometry and  $Z_{\text{rad}}(y)$  is the radiative impedance of the environment.  $E(y)$  is given by the guided mode of the slab waveguide.

To calculate the various factors in this model, we made use of three simulations. First, we determined  $L(y)$  and  $Z_{\text{rad}}(y)$  by simulating the response of a dipole current source on the interface. Next, we approximated  $\eta^2$  by simulating how strongly a dipole is excited by a plane wave incident upon an interface with different types of roughness. Finally, we calculated the modes of the structure to get the local field strength.

For the different simulations we used CAMFR,<sup>7,8</sup> a vectorial eigenmode expansion tool with perfectly matched layer boundary conditions. Along the propagation axis the structure is divided into sections with a constant refractive-index profile, in which the electromagnetic field is expanded into the local eigenmodes. Radiation modes are supported through perfectly matched layer absorbing boundary conditions. At the interface between sections, mode matching is used to decompose the field into the eigenmodes of the new section. In this way, a scattering matrix that describes the entire structure is obtained.

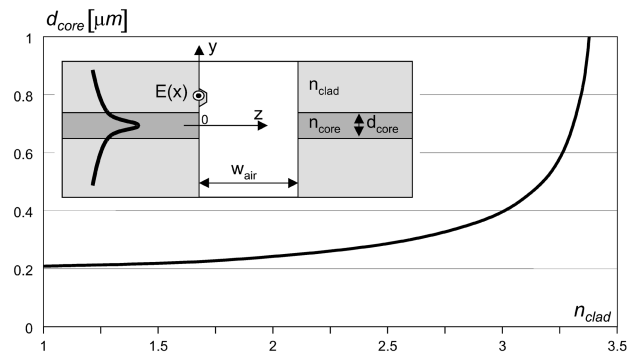


Fig. 1. Geometry of an air slot with roughness in a slab waveguide. Waveguide core width  $d_{\text{core}}$  changes with cladding index  $n_{\text{clad}}$  for a constant  $v$  number.

To compare slabs with different vertical index contrasts we used three-layer symmetric slab waveguide with a  $v$  number of 2.79 to guarantee single-mode behavior. The  $v$  number is related to the refractive-index contrast and the thickness of the waveguide:

$$v = k_0 d_{\text{core}} \sqrt{n_{\text{core}}^2 - n_{\text{clad}}^2}. \quad (3)$$

To keep the  $v$  number constant we increase core thickness  $d_{\text{core}}$  with cladding index  $n_{\text{clad}}$ , as illustrated in Fig. 1. For compatibility with both GaAs/AlGaAs and silicon-based structures, a value of  $n_{\text{core}} = 3.45$  was chosen as the index of the core. For the numerical results presented here we used an air gap of  $w_{\text{air}} = 280$  nm.

In the TE polarization, a 2-D dipole upon an interface radiates in all directions. To calculate the fraction of the dipole's power that is recaptured by the waveguide we excited a dipole by a known dipole current source  $I_0$  at position  $y$ . The power  $P_0(y)$  emitted by this source is

$$P_0(y) = \frac{I_0 E_0(y)}{2}, \quad (4)$$

where  $E_0(y)$  is the electric field measured at the position of the current source. As this is a 2-D simulation,  $P_0$  is measured in watts per meter. Likewise, the radiative impedance of the environment without roughness,

$$Z_{\text{rad},0}(y) = \frac{E_0(y)}{I_0}, \quad (5)$$

is expressed in ohms per meter.  $E_0(y)$  can be calculated in CAMFR. We found that  $Z_{\text{rad},0}(y)$  oscillates gently with  $y$ , and the oscillation is stronger for higher index contrast.

Because in a photonic crystal the forward and backward propagating light is coupled, the recaptured light in both the forward and the backward slab modes can be considered not lost. The fraction of the lost light  $L(y)$  of the dipole can therefore be expressed as

$$L(y) = \frac{P_0(y) - R(y) - T(y)}{P_0(y)}, \quad (6)$$

where  $R(y)$  and  $T(y)$  are, respectively, the power in the forward and backward propagating guided slab modes. Figure 2 shows  $L(y)$  for several values of  $n_{\text{clad}}$ . If the dipole is located near the slab core, a larger fraction of light is recovered. Also, a slab waveguide with high vertical index contrast can recapture more light because of its higher numerical aperture.

We then calculate the excitation of the dipole,  $\eta^2$ , by the incident field. It is obvious that the amount of scattering depends strongly on the type of irregularity and on the index contrast  $\Delta\epsilon_h = n_{\text{mat}}^2 - 1$  of the sidewall, where  $n_{\text{mat}}$  is the index of the material at position  $y$ . We calculate  $\eta^2$  by scattering a plane wave off a rectangular irregularity on a material-air interface and do this for different irregularities and values of  $\Delta\epsilon_h$ . Figure 3 shows  $\eta^2$  as a function of  $\Delta\epsilon_h$  for irregularities of several widths and depths. We found that  $\eta^2$  behaves much as

$$\eta^2 = \gamma(\Delta\epsilon_h)^2, \quad (7)$$

where  $\gamma$  describes the influence of the shape and size of the irregularities. This result has also been reported in the literature for orthogonal incidence.<sup>9</sup>

Now that we know  $\eta^2$  we can calculate the excitation  $P(y)$  of the dipole in an irregularity at position  $y$  by approximating  $Z_{\text{rad}}(y)$  by  $Z_{\text{rad},0}(y)$  of the unperturbed structure:

$$P(y) \cong \gamma[\Delta\epsilon_h(y)]^2 \frac{E^2(y)}{2Z_{\text{rad},0}(y)}. \quad (8)$$

Note that  $\Delta\epsilon_h$  is dependent on position  $y$ , as the index contrast of the material-air interface is higher in the slab core than in the slab cladding. Therefore, as core index  $n_{\text{core}}$  is fixed at 3.45, a low vertical index contrast implies a high value of  $\Delta\epsilon_h$  in the slab cladding. Figure 4 shows  $P(y)$  normalized to the power of the incident slab waveguide mode for several values of  $n_{\text{clad}}$ , where  $E(y)$  is based on the guided slab mode. Overall, the excitation of the dipole is much stronger for low vertical index contrasts (high values of  $n_{\text{clad}}$ ) because the mode profile is much broader and  $\Delta\epsilon_h$  in the cladding is much larger.

We now combine the results to estimate the average losses that are due to roughness by filling in all factors in Eq. (1). Figure 5 shows  $L_{\text{tot}}$  as a function of  $n_{\text{clad}}$ . There is a strong increase of losses for higher

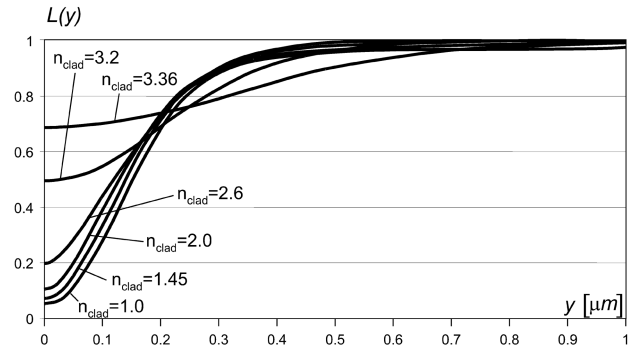


Fig. 2. Loss of a radiation dipole as a function of position  $y$ .  $L(y)$  is the fraction that cannot be recaptured by the waveguide.

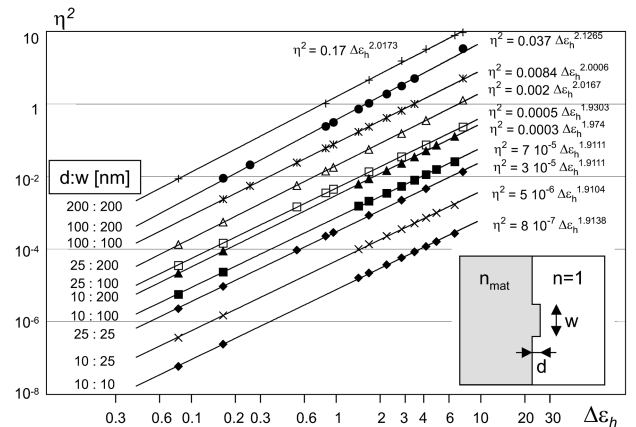


Fig. 3. Strength of a dipole excited by a plane wave incident upon an irregularity on a material-air interface, plotted as a function of material refractive index  $\Delta\epsilon_h$  for several shapes of irregularities.

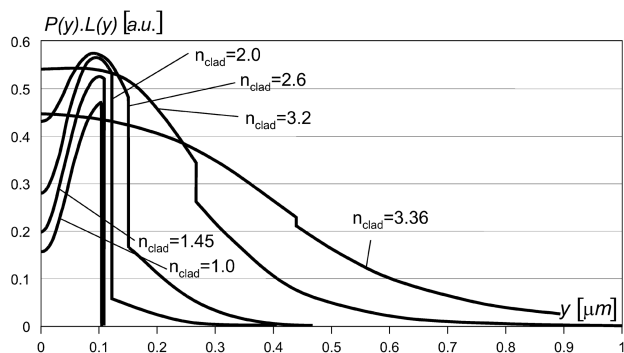


Fig. 4. Lost power  $P(y)L(y)$  of a dipole at position  $y$  excited by the slab waveguide mode incident upon single air slot. The discontinuities occur at the core-cladding interface.

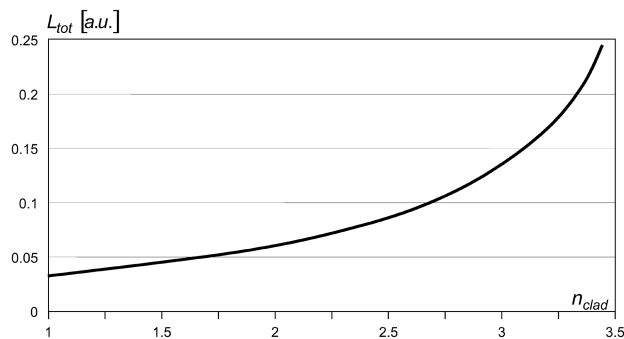


Fig. 5. Average power lost as a result of scattering at irregularities on the sidewall of a single air slot as a function of slab cladding index  $n_{\text{clad}}$ .

values of  $n_{\text{clad}}$ , i.e., for materials with lower vertical index contrasts. We can therefore conclude that high vertical-index contrast (such as in silicon-on-insulator or semiconductor membranes) performs better with respect to losses at irregularities than low out-of-plane contrast such as in GaAs/AlGaAs waveguides). This finding can provide an explanation for the discrepancy in performance between current photonic crystal

waveguides in silicon-on-insulator and in III–V semiconductors.<sup>10,11</sup> The high vertical index contrast provides a stronger confined mode, which results in a less-roughened surface and a slab with a higher numerical aperture, which collects more scattered light.

Parts of this research were carried out in the context of the European IST-PICCO project and of the Belgian Interuniversity Attraction Pole PHOTON network. W. Bogaerts thanks the Flemish Institute for the Industrial Advancement of Scientific and Technological Research for a specialization grant. P. Bienstman acknowledges a postdoctoral fellowship from the Flemish Fund for Scientific Research. W. Bogaerts's e-mail address is wim.bogaerts@intec.rug.ac.be.

## References

1. T. F. Krauss, R. M. De La Rue, and S. Brand, *Nature* **383**, 699 (1999).
2. H. Bénisty, C. Weisbuch, D. Labilloy, M. Rattier, C. J. M. Smith, T. F. Krauss, R. M. De La Rue, R. Houdre, U. Oesterle, C. Jouanin, and D. Cassagne, *J. Lightwave Technol. Lett.* **17**, 565 (2001).
3. W. Bogaerts, P. Bienstman, D. Taillaert, R. Baets, and D. De Zutter, *IEEE Photon. Technol. Lett.* **13**, 565 (2001).
4. E. Chow, S. Y. Lin, S. G. Johnson, P. R. Villeneuve, J. D. Joannopoulos, J. R. Wendt, G. A. Vawter, W. Zubrzycki, H. Hou, and A. Alleman, *Nature* **407**, 983 (2000).
5. H. Bénisty, D. Labilloy, C. Weisbuch, C. J. M. Smith, T. F. Krauss, D. Cassagne, A. Béraud, and C. Jouanin, *Appl. Phys. Lett.* **76**, 532 (2000).
6. W. Bogaerts, P. Bienstman, D. Taillaert, R. Baets, and D. De Zutter, *Opt. Quantum Electron.* **34**, 195 (2002).
7. P. Bienstman and R. Baets, *Opt. Quantum Electron.* **33**, 327 (2001).
8. CAMFR website: <http://camfr.sourceforge.net>.
9. T. A. Germer, *Appl. Opt.* **36**, 8798 (1997).
10. M. Notomi, A. Shinya, K. Yamada, J. Takahashi, C. Takahashi, and I. Yokohama, *IEEE J. Quantum Electron.* **38**, 736 (2002).
11. A. Talneau, L. Le Gouezigou, and N. Bouadma, *Opt. Lett.* **26**, 1259 (2001).